

# MOLECULAR DYNAMICS SIMULATIONS OF THERMAL CONDUCTIVITY OF PENTA-GRAPHENE

ISYNA MUNA AND SZYMON WINCZEWSKI

*Faculty of Applied Physics and Mathematics,  
Gdansk University of Technology  
Gabriela Narutowicza 11/12, 80-233 Gdansk, Poland*

(received: 2 April 2020; revised: 10 May 2020;  
accepted: 3 June 2020; published online: 1 July 2020)

**Abstract:** The thermal conductivity of penta-graphene (PG), a new two dimensional carbon allotrope and its dependence on temperature, strain, and direction are studied in this paper. The thermal conductivity of PG is investigated using a non-equilibrium molecular dynamics simulation (NEMD) with the Two Region Method by applying the optimized Tersoff interatomic potential. Our study shows that the thermal conductivity of PG (determined for the [100] direction) at the room temperature of 300 K is about 18.7 W/(m K), which is much lower than the thermal conductivity of graphene. As the temperature increases, the thermal conductivity of PG is decreasing because, unlike graphene, PG has lower phonon group velocities and few collective phonon excitations. The obtained dependence of the thermal conductivity on the temperature can be described as  $\kappa \sim T^{-0.32}$ . For the [110] direction the thermal conductivity at the room temperature of 300 K is very similar: about 17.8 W/(m K). In this case, the temperature dependence follows the  $\kappa \sim T^{-0.3}$  relation. Our investigations reveal that the thermal conductivity of PG is isotropic, meaning that heat transport behavior is independent of the heat flow direction. Our results indicate that the thermal conductivity of PG depends in an interesting way on the applied strain: nonmonotonic up-and-down behavior is observed. The thermal conductivity increases between strains from 0% up to 12.5%, and it decreases above a strain of 12.5%. Our investigation highlights the fascinating thermal transport properties of penta-graphene. The ultra-low thermal conductivity, the decreasing thermal conductivity with the increasing temperature, and the ultra-high mechanical strength of PG show that PG possesses a great potential in thermoelectric and nanomechanics applications. We hope that these findings, made by means of simulations, will become a bridge to inspire and encourage the experimental works, especially in the synthesis of PG.

**Keywords:** penta-graphene, thermal conductivity, molecular dynamics

**DOI:** <https://doi.org/10.17466/tq2020/24.3/a>

## 1. Introduction

Carbon is one of the most abundant elements by mass in the universe along with hydrogen, helium, and oxygen. Carbon atoms can bond together in various ways, forming a wide range of allotropes. This makes carbon one of the most versatile elements. The well-known carbon allotropes such as graphite, diamond, fullerene [1] (3D), nanotube [2] (1D), and graphene [3] (2D) have been discovered and researched to have outstanding properties and a good use in a wide variety of electronic and mechanical applications.

In recent years, the study of two dimensional (2D) materials, particularly the graphene, has been one of the most exciting and valuable areas in material science. Penta-graphene (PG), a latest 2D carbon allotrope has been proposed and confirmed to be dynamically and mechanically stable [4]. Contrary to most carbon allotropes with hexagonal building structures, penta-graphene is composed entirely of carbon pentagons resembling the Cairo pentagonal tiling. Many scientists have investigated many superior properties of penta-graphene. Compared to the zero band gap of graphene, PG possesses an intrinsic electronic band gap of around 3–4 eV [4, 5]. Its electric properties also can be fine-tuned by applying stacking [6, 7], doping [8, 9], or by functionalization [9, 10], make it even a more promising material.

Furthermore, penta-graphene is predicted to exhibit an unusual negative Poisson's ratio and an ultrahigh mechanical strength by being able to withstand strains as high as 25% outperforming graphene due to its unique atomic configuration [4]. Having these fascinating properties, it has been demonstrated that penta-graphene is expected to be a great candidate for broad applications in nano-electronics, nanomechanics [4], nanotransistors [11], and Li/Na-ion batteries [12].

To make full use of penta-graphene as a material in applications of future nanodevices, scientists also need to know its thermal transport (heat transfer) properties as an essential aspect beside the electric and mechanical properties. Previous research has shown that graphene has received a huge amount of attention due to its extremely high thermal conductivity at room temperature (above 3000 W/m K) [8]. Moreover, state-of-the-art theoretical calculations confirm that PG is not only dynamically and mechanically stable, but also can withstand temperatures as high as 1000 K [4].

The thermal transport properties of PG have been presented by Xu [13], who studied the importance of the structure-property relationship and probed the temperature dependence of the thermal conductivity of penta-graphene. A high thermal conductivity is necessary to remove heat, reduces the damage to the device from the Joule heating. On the contrary, low thermal conductivity is needed to increase the figure of merit in thermoelectric applications [13].

The thermal transport properties of penta-graphene were also investigated by Sun [14] merely a year ago. He has shown that the strain dependence of the thermal conductivity on monolayer PG exhibits a robust nonmonotonic up-and-down

trends. Therefore, it is necessary to understand the unexplored thermal transport property of penta-graphene so that it will create more possibilities to better functionalize penta-graphene based nanodevices.

Due to their extremely small size, the thermal conductivities of carbon nanostructures are hard to measure experimentally. Instead computer simulations are used to probe single atomic structures in a controlled and reproducible environment. Xu's investigation applied the equilibrium molecular dynamics (EMD) and the Green-Kubo formalism to predict the thermal conductivity of penta-graphene. EMD is used when the atomic vibrations of the system follow the phonon modes in the system. Additionally, despite such a significant expansion of knowledge, Sun's research on the thermal conductivity of monolayer penta-graphene under some strains has not completely pictured the variability of thermal properties of PG because he considered only five different strains varying from 0% to 13.5%. Moreover, in his work, the dependence of the thermal conductivity on the direction was not studied.

In this paper, we would like to investigate the calculation of the thermal conductivity of penta-graphene using the computational method of non-equilibrium molecular dynamics (NEMD) simulations. The NEMD is based on time reversible equations of motion and its new key idea was to replace the external thermodynamic environment by internal control variables. The new variables can control temperature, or pressure, or energy, or stress, or heat flux and maintain nonequilibrium states [15].

Furthermore, the goal is to see how the thermal conductivity depends on

1. the varying temperatures from 150 K to 900 K increased by 150 K,
2. the different strains from the initial size to 20% increased by 2.5%,
3. the direction of measurement, two crystallographic directions (namely [100] and [110]) were considered.

This paper is organized as follows. In Section 2, we provide basic information about penta-graphene, the interatomic potential, the thermal transport properties formula and the methodology used. In Section 3, we explain the simulation details and the method of analysis. In Section 4, we investigate the influence of the temperature, strain, and the direction on the thermal conductivity of PG, presenting the results of NEMD simulations. Finally, conclusions are presented in Section 5.

## 2. Theory

### 2.1. Penta-graphene

The crystal structure of penta-graphene has been described by Zhang [4] and is shown in Figure 1. PG has a tetragonal structure with the optimized lattice constant  $a = b = 3.64 \text{ \AA}$ . Each unit cell (UC) has a layered structure containing six atoms (two  $sp^3$ - and four  $sp^2$ -hybridized carbon atoms denoted as C1 and C2). In contrast to the perfectly planar graphene, it can be seen from the side view of PG (Figure 1) that there is an interlayer buckling where C1 atoms are

situated in the middle layer with  $z = 0$  whilst C2 atoms are in the upper and lower layers with  $z = \pm h$ . Here,  $h$  denotes the interlayer spacing which equals  $0.6 \text{ \AA}$ , leading to a 2D sheet with a total thickness of  $1.2 \text{ \AA}$ .

In PG the carbon-carbon bonds have the lengths  $d_1 = 1.55 \text{ \AA}$  (all C1-C2 bonds) and  $d_2 = 1.34 \text{ \AA}$  (all C2-C2 bonds). The interior bond angles of pentagons are equal to  $113.5$  (C1-C2-C2 angle, occurs twice),  $112.4$  (C1-C2-C1 angle) and  $\alpha = 98.6$  degrees (C2-C1-C2 angle, also occurs twice). There is also another C2-C1-C2 angle, which measures the wrinkles of the PG structure. According to Ref. [4] it is equal to  $\beta = 134.4$  degrees, indicating the distorted  $sp^3$  nature of C1 atoms. One unit cell of PG contains 3 atom types (shown as red, blue, and yellow color in the figure) with 2 atoms for each type.

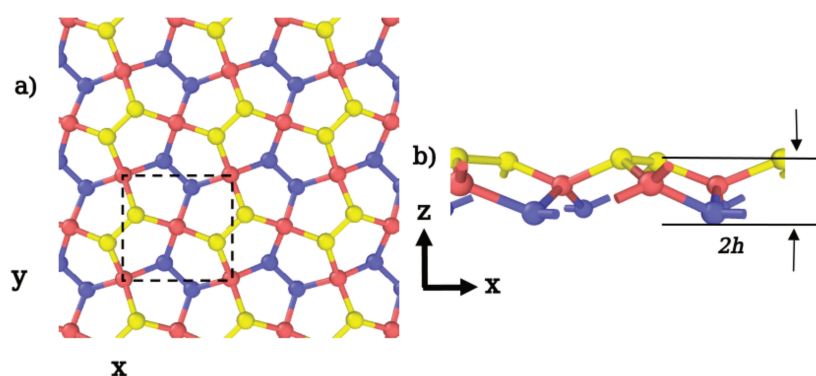


**Figure 1.** Structure of penta-graphene: top (panel a) and side (panel b) views. The  $sp^3$ -hybridized atoms (C1) are shown in red, while the  $sp^2$ -hybridized atoms (C2) are shown in blue (lower layer with  $z = -h$ ) and yellow (upper layer with  $z = +h$ ). The illustration was prepared using OVITO [16].

In this work, we also investigate the structure of PG rotated by  $45$  degrees, such that the coordinate  $x$ - and  $y$ -directions correspond to the  $[110]$  crystallographic direction. The bond length of all C1-C2 and C2-C2 bonds remains the same as its initial (non-rotated) structure. One unit cell of a rotated structure of PG contains three atom types (shown as red, blue, and yellow in the figure) with 4 atoms for each type.

## 2.2. Tersoff Potential

The important key to accurately examine results from MD simulations is by choosing the proper interatomic potential. In the previous research [17], it has been shown that there is only one potential which correctly describes all the important features of PG among empirical potentials available for the elemental carbon, namely a new parameterization of the Tersoff potential [18, 19] proposed by Erhart and Albe in 2005 [20]. This potential reproduces the structure of PG

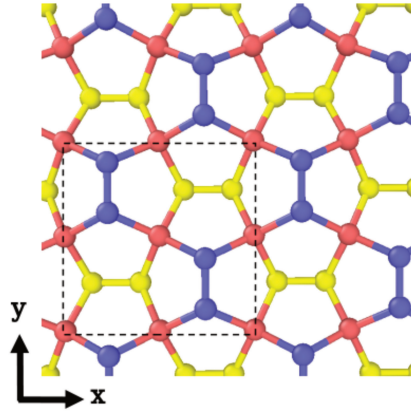


**Figure 2.** Structure of PG oriented such that x- and y- coordinate directions correspond to [110] directions

and its linear mechanical properties very well. At the same time it also provides a reliable picture of the thermodynamic stability of PG [17].

As for an empirical model, this potential also convincingly describes the nonlinear mechanical behavior of PG, even at strains as high as 0.2. Therefore, in this work we have employed this potential to describe the interactions of carbon atoms in PG [21].

The formula of the total potential energy  $U_{tot}$  of the system composed of  $N$  atoms within the Tersoff potential is given by:

$$U_{tot} = \sum_i \sum_{j>i} f_c(r_{ij}) \left[ V_R(r_{ij}) - \frac{b_{ij} + b_{ji}}{2} V_A(r_{ij}) \right] = \sum_i \sum_{j>i} V_{ij} \quad (1)$$

Here,  $r_{ij}$  denotes the distance between atoms  $i$  and  $j$ . The functions  $V_R(r)$  and  $V_A(r)$  describe the repulsion and attraction and both have an exponential form. The factor  $b_{ij} = (b_{ij} + b_{ji})/2$  which occurs before the second term is the bond order.

By scaling the attractive term  $V_A$  it controls the bond strength, enabling a simultaneous (*i.e.* obtained within one approach) description of single, double and triple covalent bonds. The  $b_{ij}$  parameter depends on the configuration of the system in the vicinity of atoms  $i$  and  $j$ . This causes the Tersoff potential to be, in fact, a many-body potential [22].

The cut-off function  $f_c(r)$  smoothly turns off the interactions between distant atoms, causing that it is only the contributions of pairs of atoms which are covalently bonded that are included in the double summation present in the previous equation. The cut-off formula is given by:

$$f_c(r_{ij}) = \begin{cases} 1, & \text{if } r_{ij} < R - D \\ \frac{1}{2} - \frac{1}{2} \sin\left(\frac{\pi}{2} \frac{r_{ij} - R}{D}\right), & \text{if } R - D \leq r_{ij} \leq R + D \\ 0, & \text{if } r_{ij} > R + D \end{cases} \quad (2)$$

Here, the parameters  $R$  and  $D$  determine the region in which the cut-off function approaches zero. It is possible to consider the  $V_{ij}$  contribution to be energy associated with the  $i-j$  bond. However, it must be stressed here that the  $V_{ij}$  contribution defined in this way is not a two body contribution, as it depends also on the positions of atoms which are nearest neighbors of atoms  $i$  and  $j$ , through the bond order  $b_{ij}$ . In fact, the  $V_{ij}$  term describes not only the energetics of the bond stretching, but also captures all the bond-bond effects that occur when the valence angle between two adjacent bonds is varied.

There are eleven parameters for the Tersoff potential the values of which are taken from the paper of Erhart and Albe [20]. All the parameters are given in Table 1.

**Table 1.** Parameters of the optimized Tersoff potential used to describe interatomic interactions in penta-graphene

| Parameters                        | C          |
|-----------------------------------|------------|
| $A$ (eV)                          | 2019.8449  |
| $B$ (eV)                          | 175.426651 |
| $\lambda_1$ ( $\text{\AA}^{-1}$ ) | 4.18426232 |
| $\lambda_2$ ( $\text{\AA}^{-1}$ ) | 1.93090093 |
| $\lambda_3$ ( $\text{\AA}^{-1}$ ) | 0.0        |
| $R$ ( $\text{\AA}$ )              | 2.0        |
| $D$ ( $\text{\AA}$ )              | 0.15       |
| $m$                               | 1.0        |
| $n$                               | 1.0        |
| $c$                               | 181.91     |
| $d$                               | 6.28433    |
| $\cos(\theta_0)$                  | -0.5556    |
| $\beta$                           | 1.0        |
| $\gamma$                          | 0.11233    |

### 2.3. Thermal Conductivity

Thermal conductivity ( $\kappa$ ) is the ability of a given material to transport/conduct heat. It represents the amount of the thermal energy which flows per unit time through a unit area with a temperature gradient of one degree per unit distance. Thermal conductivity is an important physical phenomenon to dissipate the formed thermal energy in a system. Macroscopically, thermal conductivity is calculation of the propensity of a material to transmit heat energy in a diffusive manner as given by

$$J_x = -\kappa \frac{\partial T}{\partial x} \quad (3)$$

where  $J_x$  is the heat flux, while  $\partial T/\partial x$  is the temperature gradient along the heat transport direction. The thermal conductivity ( $\kappa$ ) has units of energy per distance per time per degree K (W/(m K)) [23].

The thermal conductivity of penta-graphene will be calculated via non-equilibrium molecular dynamics simulations (NEMD) using the so-called “Two-Region Method” illustrated in Figure 3 (a detailed step-by-step description will be provided in the next section).

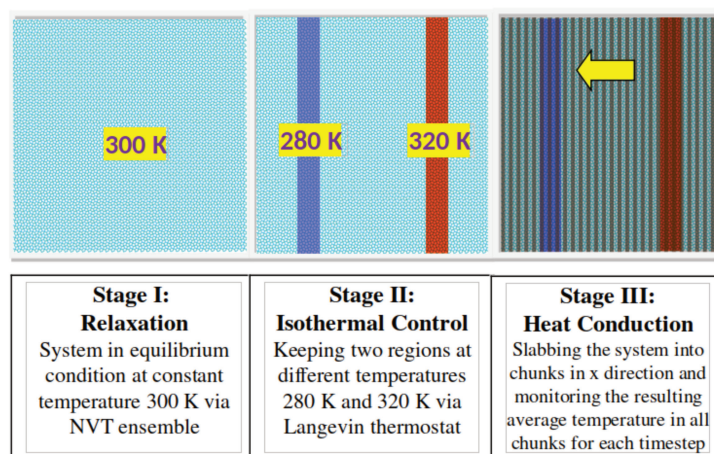


**Figure 3.** The three stages of performing NEMD simulation of heat transport at temperature 300 K using Two Region Method

#### 2.4. Simulation Protocols

This paper is aimed to calculate the thermal conductivity of PG via non-equilibrium molecular dynamics simulations (NEMD). The NEMD is chosen to simulate the system from an isobaric-isothermal ensemble (NPT) and needs longer time of running. Unlike MD simulations that can obtain  $\kappa$  values directly from the output file (.log) as heat flux since the fluctuations of the per-atom potential, kinetic energies, and stress tensor are calculated in a steady-state equilibrated simulation; in NEMD,  $\kappa$  will also be computed from the additional output file as the temperature profile (.profile). The temperature profile will monitor the continuous flow of energy between hot and cold regions of the simulation box.

We used the LAMMPS software to perform the non-equilibrium MD simulation. The name stands for “Large-scale Atomic/Molecular Massively Parallel Simulator”. It is an open-source code developed by the Sandia National Laboratories designed to perform molecular dynamics simulations with special focus on material modeling. LAMMPS has a great potential for solid-state materials (metals, semiconductors) and can be used to model atoms or as a parallel particle simulator at the atomic and continuum scale [23].

In this paper, the NEMD simulation consists of two parts. The first part is the initial simulation which is used to obtain the lattice parameters of a PG structure and a rotated PG structure from the equilibrated simulation system. The second part are the main simulations which will calculate the thermal conductivity of PG depending on the temperature, strain, and direction.

Before running each simulation with LAMMPS, we need to create an input file using a text editor such as Vim with all the commands LAMMPS needs to execute. There are two other files that will be needed to run the input file, such as the data file and the parameter file. The data file is read into LAMMPS with the *read\_data* command and contains the basic information about the size of the problem to be run, the initial atomic coordinates, and the molecular topology.

The parameter file contains the parameters of the chosen interatomic potential and is used by the *pair\_coeff* command. LAMMPS has a built-in library of interatomic models with parameters for a list of selected materials. Since we are interested in parameterization by Erhart and Albe [20], in this report we use the Tersoff potential for describing interactions and they are all found in the LAMMPS library. In the next section, we will show excerpts of such an input file and explain the commands essential for our studies.

The carried out simulation will give some output files depending on the written commands. In our work, we have three outputs such as log, profile and dump (lammprj) files. The log file contains the temperature, pressure, volume, and potential energies at each timestep. We use the open-source program Ovito and VMD [16, 24] to visualize all the data. The software allows us to investigate the output data by examining the penta-graphene at every timestep to visually determine the thermal expansion behavior.

We use the Gnuplot program which is an open source and portable command-line driven graphing utility for plotting, fitting, and various computations. It was created in 1986 and has been used by scientists and students to visualize mathematical functions and data interactively [25].

The entire simulation consists of three stages that are presented in Figure 4. In Stage I, the system is thermalized for a given temperature. This is done by means of a simulation carried out in the NVT ensemble. In Stage II, a temperature gradient is applied and the system is further equilibrated. In this stage, the temperature of two special regions (left and right, cold and hot) is controlled by means of the Langevin thermostat. After the system has been successfully equilibrated and reached the steady-state in Stage II, in the subsequent Stage III we continue to control the temperature in two special regions. In this stage the equilibrated system is sampled, by monitoring the temperature gradient between two special regions. The energies added/removed by two thermostats are also monitored.



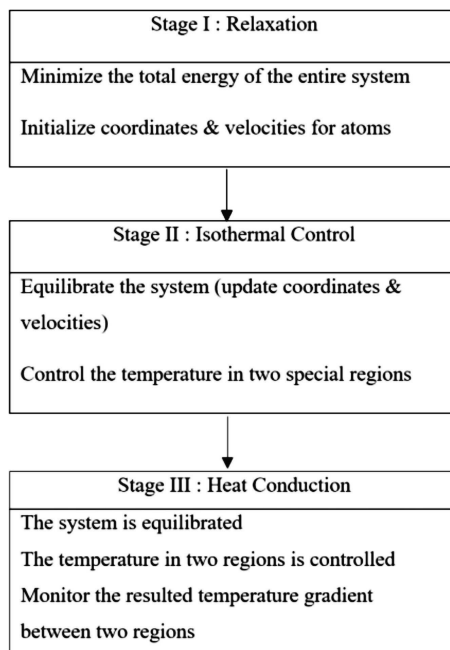


Figure 4. Flowchart showing the the numerical simulation structure used in this paper

### 3. Method

In the following section, we are going to explain the most essential parts of the input file used in the simulation and provide an example of a full input file in Appendix A. Please note that lines starting with “#” are not read by LAMMPS and are intended to make the file more easily understood by the reader. The method will be divided into two parts, the initial simulation and main simulations.

#### 3.1. Initial simulation

As we have mentioned earlier in the foregoing Subsection 2.4, the initial simulation is used to obtain the equilibrium lattice parameters of penta-graphene for various temperatures. The input file starts by defining the units used, the dimensionality (3D), and the boundary conditions, as shown in the box below. We choose periodic boundary conditions only in two directions of  $x$  and  $y$  while in  $z$  direction we set a fixed (non-periodic) boundary condition. This will allow us to perform the isobaric-isothermal relaxation later.

```

-----
dimension      3
boundary       p p f
units          metal
atom_style     atomic
-----
  
```

Next, we define the interatomic potential used (set to *tersoff*) in the *pair\_style* command. A single *pair\_coeff* command is used to specify the parameters for all the needed elements in the Tersoff potential which is written in a file named *penta.tersoff*. After that,  $N$  additional arguments are specified to map the elements into atom types. Since penta-graphene consists of three types of carbon atoms, hence the  $N$  arguments are C C C. We also define the atom types and the mass of the chosen elements.

```
-----
pair_style      tersoff
pair_coeff      * * penta.tersoff C C C

mass           1 12.0
mass           2 12.0
mass           3 12.0
-----
```

Then, we also need to read a file which contains the initial positions of atoms. This is done using *read\_data* command.

```
-----
read_data      penta_graphene.data
-----
```

In the section below we aim to minimize the energy of the system with an equilibration step. We will be thermostating and barostatting the system in the in-plane sizes because it is a quasi-2D system. The thermostating and barostatting are achieved by adding some dynamic variables which are coupled to the particle velocities (thermostating) and simulation domain dimensions (barostatting).

The fix of the *npt* style performs the time integration sampled from the isothermal-isobaric (NPT) ensemble and updates the positions and velocities of atoms. We choose a rather small timestep of 0.5 femtosecond.

In thermostating, the *temp* keyword is used to specify the thermostat parameters. *Tstart*, *Tstop* are the external temperatures at the start or end of a run and *Tdamp* is the temperature damping parameter in time units that determines how rapidly the temperature is relaxed. In this simulation, we set *Tstart* and *Tstop* to 150 K. As suggested in the LAMMPS manual, a good choice for *Tdamp* is around 100 timesteps and we take 200 timesteps as *Tdamp*. Since our timestep is 0.0005 ps (0.5 fs), then *Tdamp* should be of the order of 0.1 ps ( $200 \times 0.0005$  ps).

In barostatting, we use keywords such as *x*, *y*, and *couple* to specify the barostat parameters. The *x* and *y* keywords are used to specify the *x* and *y*

components of the stress tensor (both are set to zero). As suggested in the LAMMPS manual, the good choice for  $Pdamp$  is around 1000 timesteps and we take 2000 timesteps as  $Pdamp$ . Since our timestep is 0.0005 ps (0.5 fs) then  $Pdamp$  should be of the order of 1.0 ps ( $20000 \times 0.0005$  ps). Moreover, the *couple* keyword is set to *none*. This causes that each dimension will be controlled independently.

A random number generator assigns initial velocities to the atoms. These velocities are generated from a uniform distribution and are scaled to match the specified temperature, here: 150 Kelvin. The generator uses the same seed (12345) for all simulations. In addition, the total linear and angular momenta of the generated ensemble of velocities are zeroed.

```
-----
fix          1 all npt temp 150.0 150.0 0.1 &
             x 0.0 0.0 1.0 &
             y 0.0 0.0 1.0 &
             couple none
timestep     0.0005
velocity     all create 150.0 12345 rot yes mom yes
-----
```

The *thermo* command is used for printing the thermodynamic info, such as temperature, energy, and pressure on timesteps that are a multiple of  $N$  (here, 100) and at the beginning and end of a simulation. In the *thermo\_style* command, the *custom* style is used to specify which of the thermodynamic parameters will be printed.

The *custom* style in the *dump* command allows us to specify a list of atom attributes to be written to the dump file named *dump.lammpstrj*. The atom ID, atom type, and unscaled atom coordinates (*id*, *type*, *x*, *y*, and *z*) will appear in the specified order. Dumps occur at the very end of a timestep, hence, atom attributes will include effects due to fixes that are applied during the timestep. Only the information for atoms in the specified group is dumped and dump files can be read directly by OVITO, a popular molecular viewing program.

```
-----
thermo_style  custom step temp press lx ly
thermo       100
dump         myDump all custom 100 dump.lammpstrj.* id type x y z
-----
```

Once we run the above simulations, we will obtain (for each considered temperature) the output file named *log.lammps*. Its columns contain the values of *step*, *temp*, *press*, *lx*, and *ly*. Then we manage only the column of system size  $L_x$  to be included in the determination of the lattice parameter. To obtain the lattice

parameter  $a$ , firstly we calculate the average  $L_x$  for each temperature (150 K, 300 K, ..., 900 K) and then divide it by the number of repetitions of the unit cell  $nx$  (in this case 10).

Next, to see how  $a$  depends on the temperature  $T$  such that we are able to account for the thermal expansion, we plot the obtained values of average  $L_x$  as a function of the temperature, and fit it with a linear function using GNUplot. The fitted function is given by  $a = AT + B$ , where  $A$  and  $B$  are the fit coefficients. Knowing the fit ( $a = AT + B$ ) we will be able to calculate the lattice parameter  $a$  for any temperature in which we are interested.

### 3.2. Initial simulation

As we have mentioned earlier in previous Subsection 2.4, the main simulations are used to perform the thermal conductivity calculation of PG which depends on **a)** temperature, **b)** strain, and **c)** direction. The thermal conductivity of PG is calculated via non-equilibrium molecular dynamics (NEMD) simulations using LAMMPS [26]. In NEMD, we imposed a temperature gradient in the system and measured the induced heat flux. The thermal conductivity can be determined by using the Fourier law. Periodic boundary conditions are applied in the in-plane directions while the free boundary condition for the  $z$  (out-of-plane) direction (see Fig. 5).

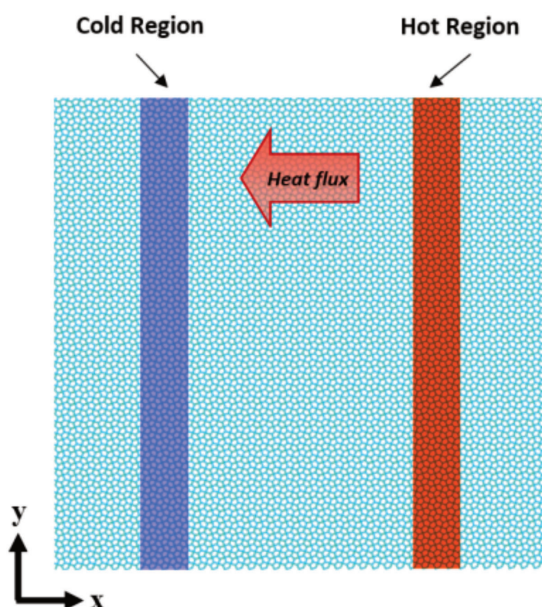


**Figure 5.** Model simulated within the Two Region Method used in the NEMD simulation



In this simulation model, the simulated system of PG has a length of 14.4 nm and a width of 14.4 nm ( $40 \times 40$  unit cells). The size of the rotated PG structure is  $14.3 \text{ nm} \times 14.3 \text{ nm}$  ( $28 \times 28$  unit cells). We will consider six different temperatures with the corresponding temperature change  $\Delta T = (T_{right} - T_{left})/2$  being proportional to  $T$  (see Table 2). Moreover, we will also study strains ranging from  $x = 0$  to  $x = 0.20$ , with the increment  $\Delta x = 0.025$ .

**Table 2.** Specification of temperatures used to investigate thermal conductivity of PG

| Temperature<br>T (K) | Change of<br>Temperature $\Delta T$ (K) | Tleft<br>(K) | Tright<br>(K) |
|----------------------|---|--------------|---------------|
| 150                  | 10                                      | 140          | 160           |
| 300                  | 20                                      | 280          | 320           |
| 450                  | 30                                      | 420          | 480           |
| 600                  | 40                                      | 560          | 640           |
| 750                  | 50                                      | 700          | 800           |
| 900                  | 60                                      | 840          | 960           |

The velocities to the atoms in the system are assigned by a random number generator. Three different seeds are used in the generation performed at different steps of the simulation. *seed\_1* will be used in the setup of initial velocities, *seed\_2* and *seed\_3* are for generating velocities in the left (cold) and right (hot) regions, respectively. We will perform five independent simulations for each temperature with five unique seeds (seed *A*, *B*, ..., *E*) in order to ascertain if the simulations are reproducible. The total linear and angular momenta of the generated ensemble of velocities are set to zero. The list of seeds used can be seen in Table 3.

**Table 3.** List of chosen seed numbers to perform simulations in our work

|        | Seed_A | Seed_B | Seed_C | Seed_D | Seed_E |
|--------|--------|--------|--------|--------|--------|
| Seed_1 | 12312  | 1      | 100    | 45     | 4000   |
| Seed_2 | 45623  | 2      | 200    | 55     | 5000   |
| Seed_3 | 78934  | 3      | 300    | 65     | 6000   |

To begin the simulation, we need to create an input file which starts with the setup of the problem. We have shown above in Subsection 3.1, how to determine the units, the dimensionality (3D), the boundary conditions, and the interatomic potential.

Next, we define 9 atom types (see the box below) since we would like to assign different names to some atoms depending to which region of the structure they belong.



```

-----
mass      1 12.0
mass      2 12.0
mass      3 12.0
mass      4 12.0
mass      5 12.0
mass      6 12.0
mass      7 12.0
mass      8 12.0
mass      9 12.0
-----

```

The three regions of the simulated system of PG are defined in the *group* command in the box below as *left* (cold region), *right* (hot region) and *centre* (remaining part of the system).

```

-----
group      left  type 4 5 6
group      center type 1 2 3
group      right type 7 8 9
-----

```

The cold region is located in the range of  $Lx/4 - D$  and  $Lx/4 + D$ , while the hot region is situated in the range of  $3Lx/4 - D$  and  $3Lx/4 + D$ . The structure of PG (with all regions highlighted) is shown in Figure 6.

In the initialization step, we generate initial velocities of all atoms in the system. The velocities are generated for the specified temperature  $T$  (150, 300, ... , 900 K) using *seed\_1*. We also define two computes which calculate the temperature of the left and right region. This is done using the *compute* command.

```

-----
velocity   all create ${t} ${seed_1} dist gaussian

compute    Tleft left  temp
compute    Tright right temp
-----

```

In what follows, we enter the main part of the Two Region Method which consists of 3 stages. We begin with the time integration. At the beginning the system is simulated in the NVT ensemble for  $n\_steps\_stage\_1$  (here, 10000) steps. The thermodynamic information (such as the temperature, energy, and pressure) is printed using the *thermo* command on every 10 timesteps ( $n\_thermo$ ). The equations of motion are integrated with a timestep of 0.5 fs (0.0005 ps) which is a standard timestep for modeling solids.



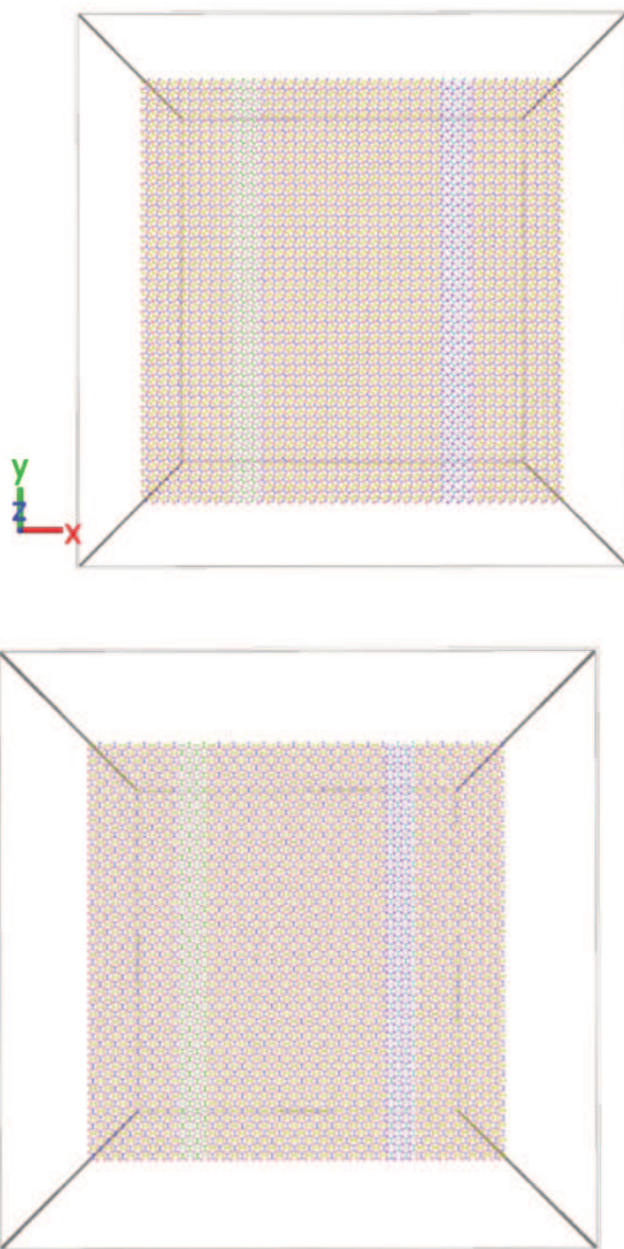


**Figure 6.** Illustration of the simulation box of the initial system in  $\langle 100 \rangle$  directions (top) and a rotated system in  $\langle 110 \rangle$  directions (bottom) with two different regions for the thermostat on the left side (green color of the cold region) the and right side (blue color of the hot region)

```

-----
# --- 1st stage ---
# 1st equilibration run

fix          nvt_fix all nvt temp ${t} ${t} ${tdamp}
thermo       ${n_thermo}
run          ${n_steps_stage_1}

timestep     0.0005
unfix       nvt_fix
reset_timestep 0
-----

```

Once this initial thermalization is completed, we impose a temperature gradient and equilibrate the system further. In this stage we control the temperature of two special regions (left and right, cold and hot) via *fixlangevin* and monitor the energy added (or subtracted) by each of two thermostats.

The width of both special regions (cold and hot reservoirs) is fully fixed, each being 10 Å (as shown in Fig. 1). The cold and hot reservoirs are coupled with independent thermostats to maintain a constant temperature in the left  $t_{lo}$  and right  $t_{hi}$  regions, respectively; while the remaining region evolves freely (without any temperature control) in the simulation. *seed\_2* and *seed\_3* are applied to generate velocities in both regions. Since the amount of added energy to the hot region is equal to the energy removed from the cold region the total energy of the system remains unchanged, resulting in a stable temperature.

The *thermo\_style* command causes that the instantaneous temperatures of two regions (global values calculated by *Tleft* and *Tright* computes), as well as other interesting quantities, will be printed on each thermodynamic timestep. The thermodynamic information (such as the temperature of two special regions, temperature of the remaining part of the system, the amount of energy added to the hot region, and the amount of energy removed from the cold region) is printed using the *thermo* command. This occurs every  $n_{thermo}$  (here, 10) steps. In the second stage the system is simulated for  $n_{steps\_stage\_2}$  (here, 50000) steps.

```

-----
# --- 2nd stage ---
# 2nd equilibration run

fix          nve_fix all nve
fix          left_thermostat left langevin ${tlo} ${tlo} ${tdamp} &
                                                    ${seed_2} tally yes
fix          right_thermostat right langevin ${thi} ${thi} ${tdamp} &
                                                    ${seed_3} tally yes
fix_modify   left_thermostat temp Tleft
-----

```



```

fix_modify      right_thermostat temp Tright

variable        tdiff equal c_Tleft-c_Tright
thermo_style    custom step temp c_Tleft c_Tright &
                f_left_thermostat f_right_thermostat v_tdiff
thermo          ${n_thermo}
run             ${n_steps_stage_2}

```

Once the system has reached a steady-state, in the last stage we still control the temperature in two special regions using *fix langevin*, similarly as it was in the previous stage. Since the third stage corresponds to sampling we collect information about the system's behavior. By using *fix ave/time*, we calculate average temperature difference. Here, we specify parameters such as *Nevery*, *Nrepeat* and *Nfreq*, which control how the averaging will be done.

The *ke/atom* compute calculates the per-atom translational kinetic energy for each atom in the system. Based on these energies temperature profile (along the heat transport direction) is computed. The entire system is divided into 80 slabs along the *x* direction. Each slab has the thickness of 1.82. The calculated per-atom energies are later reduced using *fix ave/chunk*. The accumulated average values are monitored and printed (every 1000 timesteps) to the output file named *profile.langevin*. In the third stage the system is simulated for *n\_steps\_stage\_3* (here, 100000) steps.

```

-----
# --- 3rd stage ---
# thermal conductivity calculation

# reset langevin thermostats to zero energy accumulation
unfix          left_thermostat
unfix          right_thermostat

fix            left_thermostat left  langevin ${tlo} ${tlo} ${tdamp} &
                ${seed_2} tally yes
fix            right_thermostat right langevin ${thi} ${thi} ${tdamp} &
                ${seed_3} tally yes

fix_modify     left_thermostat temp Tleft
fix_modify     right_thermostat temp Tright

fix            ave all ave/time 10 100 1000 v_tdiff ave running
thermo         1000
thermo_style   custom step temp c_Tleft c_Tright &
                f_left_thermostat f_right_thermostat v_tdiff f_ave

```

```

compute      ke all ke/atom
variable     temp atom c_ke/(1.5*${kB})
compute      layers all chunk/atom bin/1d x lower 1.82 units box
fix          temp_profile all ave/chunk 10 100 1000 layers &
                                                    v_temp file profile.langevin

run          ${n_steps_stage_3}

```

---

## 4. Results

### 4.1. Temperature dependence of thermal conductivity of penta-graphene

#### 4.1.1. Lattice Parameter

After running the initial simulations (which served to determine the lattice parameter) we create a plot which shows how the lattice constant  $a$  depends on the temperature (see Figure 7, raw results are shown in Table 4). Additionally, we also plot the fitted linear function of the form  $a = AT + B$ , where  $A$  and  $B$  are fit coefficients. The plot illustrates how the lattice constant  $a$  depends on temperature  $T$ ; and shows that PG is characterized by a positive thermal expansion, in contrast to graphene which has an unusual negative thermal expansion.

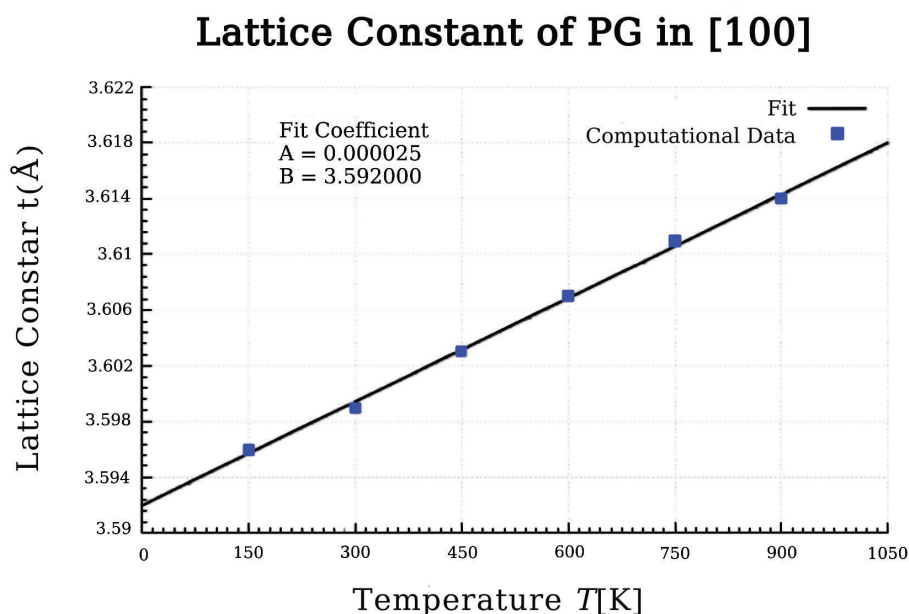


**Figure 7.** Lattice constants  $a$  of PG in [100] direction plotted using *GNUplot*. Coefficients  $A = 0.000025$  and  $B = 3.592000$

**Table 4.** List of equilibrium lattice constants  $a$  of PG for different temperatures

| Temperatures<br>(K) | Lattice Constants<br>(Å) |
|---------------------|--------------------------|
| 150                 | 3.5958                   |
| 300                 | 3.5995                   |
| 450                 | 3.6032                   |
| 600                 | 3.607                    |
| 750                 | 3.6108                   |
| 900                 | 3.6145                   |

Knowing the fitted function ( $a = 0.000025T + 3.592000$ ) we are able to calculate the lattice constant  $a$  for any temperature in which we are interested.

#### 4.1.2. Calculation of thermal conductivity $\kappa$

In the following section, we calculate the thermal conductivity ( $\kappa$ ) of penta-graphene and investigate its temperature dependence. The thermal conductivity was calculated based on NEMD simulations combined with the Two Region Method. The simulated system (penta-graphene sheet) consisted of 40 x 40 repetitions of the six-atom unit cell (14.4 nm x 14.4 nm). We chose the temperature of 300 K with seed  $A$  as a simulation example to be shown in this work. Additionally, in Table 5 we also present a complete calculations for other runs (and other seeds) which were carried out for temperature 300 K.

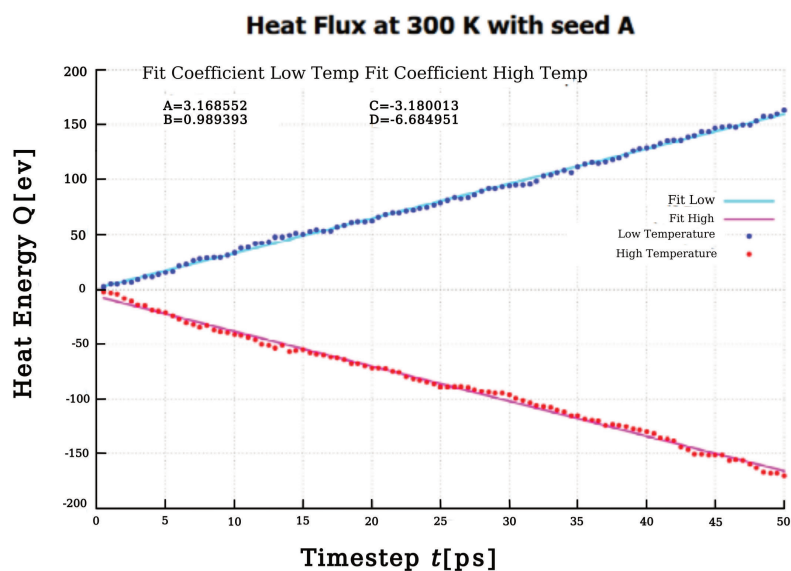
The thermal conductivity ( $\kappa$ ) of penta-graphene is determined by using Fourier's Law as

$$\kappa = -\frac{J_x}{\frac{\partial T}{\partial x}} = -\frac{\left(\frac{\Delta Q}{2S\Delta t}\right)}{\frac{\partial T}{\partial x}}$$

For the calculation of heat flux  $J_x$ , we need to account for the amount of heat energy  $Q$  which flows per unit time  $t$  across the cross-sectional area  $S$  perpendicular to the transport direction. The area  $S$  is then computed from twice of  $L_y$  (since the energy flows in two directions) multiplied by thickness  $h$  of penta-graphene. We consider  $h$  to be 4.6 Å and it can be taken by the *vdW* diameter of C atom (the distance between planes in graphite) as 3.4 Å plus the buckling distance of PG (the distance between its external planes) as  $2 \cdot 0.6$  Å = 1.2 Å. As for the time, the timestep length used by us is 0.5 fs and the total time of the simulation is 50 ps. The heat flux can be determined based on the values written to the output file *file.log* (see the box below). Its columns (fifth and sixth) contain the information about the amount of heat energy added (*f\_right\_thermostat*) and removed (*f\_left\_thermostat*) to the hot region and cold region, respectively. The dependence of these energies on the simulation time is presented in Figure 8. It is visible that both dependencies are linear. The heat flux can be calculated based on the slopes ( $A$  and  $C$ ) of the fitted functions. The

**Table 5.** Example of the output file *file.log*

| Step   | Temp      | c_Tleft   | c_Tright  | f_left_thermostat | f_right_thermostat | v_tdiff    | f_ave      |
|--------|-----------|-----------|-----------|-------------------|--------------------|------------|------------|
| 0      | 298.36635 | 289.19168 | 311.15875 | -0                | -0                 | -21.967064 | 0          |
| 1000   | 298.80989 | 307.85844 | 303.31058 | 2.1269674         | -2.4717904         | 4.54786    | -20.526376 |
| 2000   | 298.7674  | 286.23169 | 296.34538 | 4.5713064         | -3.5725042         | -10.113694 | -16.137175 |
| 3000   | 295.43186 | 280.92439 | 300.33181 | 4.9291082         | -4.7213044         | -19.407421 | -14.540837 |
| ⋮      | ⋮         | ⋮         | ⋮         | ⋮                 | ⋮                  | ⋮          | ⋮          |
| 99000  | 303.32341 | 304.16568 | 309.57929 | 160.02948         | -167.78873         | -5.4136167 | -18.33819  |
| 100000 | 299.19771 | 285.03675 | 302.34804 | 162.84548         | -170.2407          | -17.311282 | -18.325791 |

**Figure 8.** Plot of heat energy with respect to timesteps at temperature 300 K with seed A. The absolute heat flux value is calculated as average of fitted coefficients A and C.

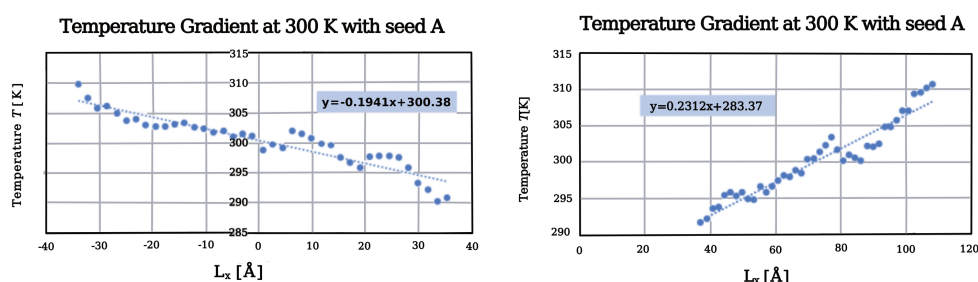
total energy remains conserved and the system temperature is rather stable at 300 K.

Next, the temperature gradient ( $\Delta T$ ) is calculated from the temperature profile written to the output file *file.profile* (example in Table 6). The calculated temperature profile is plotted and fitted with two linear functions. The fitting is performed separately in regions extending between the coordinates  $-L_x/4$  and  $L_x/4$ , and between the coordinates  $L_x/4$  and  $3L_x/4$ . The real temperature gradient is actually the average of the absolute values of the slopes of those fits (fit coefficients). The plot of the temperature gradient is presented in the Figure 9.

Having calculated the heat flux and the temperature gradient of PG at 300 K for five different seeds, we obtain the mean value of the thermal conductivity ( $\kappa$ ) as  $18.7 \pm 2.73$  W/(mK). The same steps of the thermal conductivity calculation

**Table 6.** Example of the output file *file.profile*

| Timestep | Number-of-chunks | Total-count |         |
|----------|------------------|-------------|---------|
| Chunk    | Coord1           | Ncount      | v_temp  |
| 1000     | 80               | 9600        |         |
| 1        | 0.91             | 120         | 297.752 |
| 2        | 2.73             | 120         | 301.095 |
| 3        | 4.55             | 120         | 296.526 |
| ⋮        | ⋮                | ⋮           | ⋮       |
| 79       | 142.87           | 124.07      | 300.051 |
| 80       | 144.69           | 32.05       | 299.476 |
| 2000     | 80               | 9600        |         |
| 1        | 0.91             | 120         | 312.939 |
| ⋮        | ⋮                | ⋮           | ⋮       |
| 80       | 144.69           | 29.33       | 315.531 |
| 100000   | 80               | 9600        |         |
| 1        | 0.91             | 120         | 302.856 |
| ⋮        | ⋮                | ⋮           | ⋮       |
| 80       | 144.69           | 29.91       | 300.737 |

**Figure 9.** The temperature gradient of PG at 300 K with seed A. The slope on the left is  $-0.1941$  and  $0.2312$  on the right. The temperature gradient is calculated as an absolute average of the two slopes

are applied to other temperatures from 150 K, 450 K, 600 K, 750 K, and 900 K. At room temperature 300 K, our calculated thermal conductivity of  $18.7 \pm 2.73$  W/(mK) with the effective length of 14.4 nm, width of 14.4 nm, and thickness of  $4.6 \text{ \AA}$  is much lower than  $167 \pm 3$  W/(mK) with the length of 21.84 nm, the width of 21.84 nm, and the interlayer thickness of  $4.8 \text{ \AA}$  obtained by Xu [13]. Since the system sizes used are comparable, the significant difference in the calculated thermal conductivity should be mainly attributed to different interatomic potentials used by Xu, who employed the original Tersoff potential [18], while we applied the optimized Tersoff potential to describe the interaction between carbon atoms.

**Table 7.** Detail calculations for thermal conductivity of PG at 300 K with five different seeds using Two Region Method

|                      | 300 K_A | 300 K_B | 300 K_C | 300 K_D | 300 K_E |
|----------------------|---------|---------|---------|---------|---------|
| a (Å)                | 3.5995  | 3.5995  | 3.5995  | 3.5995  | 3.5995  |
| $L_y$ (Å)            | 143.98  | 143.98  | 143.98  | 143.98  | 143.98  |
| Thickness (Å)        | 4.6     | 4.6     | 4.6     | 4.6     | 4.6     |
| Area (Å)             | 1382.21 | 1382.21 | 1382.21 | 1382.21 | 1382.21 |
| Energy Flux (eV/ps)  | 3.17428 | 3.56000 | 3.73478 | 3.75043 | 3.47328 |
| Temp. Grad. (K/Å)    | 0.2125  | 0.2184  | 0.2002  | 0.24865 | 0.279   |
| $\kappa$ (eV/ps/Å/K) | 0.011   | 0.012   | 0.014   | 0.011   | 0.010   |
| $\kappa$ (W/m/K)     | 18.030  | 19.689  | 22.533  | 18.218  | 15.037  |
| Mean $\kappa$        | 18.7    |         |         |         |         |
| St. Dev.             | 2.7     |         |         |         |         |

#### 4.1.3. Temperature Dependence on Thermal Conductivity of Penta-Graphene in [100] direction

After running all simulations and calculating the thermal conductivity of PG for each temperature, we investigate the relationship between temperature and thermal conductivity (see Figure 10). The obtained dependence of the thermal conductivity on the temperature can be described with a function of the form  $\kappa \sim T^{-0.32}$ .

From our simulations we found that penta-graphene is thermodynamically stable even at very high temperature  $T = 900$  K (see Figure 11). This result is consistent with the previous research carried out by Zhang [4], who employed ab initio molecular dynamics (AIMD) simulations.

#### 4.2. Strain Dependence on Thermal Conductivity of Penta-Graphene

Knowing the lattice constants for each temperature from Subsection 4.1, in this paper we chose to use temperature of 300 K and 600 K for investigating the strain dependence of the thermal conductivity. We considered various strains from  $x = 0$  to  $x = 0.20$ , with the increment  $\Delta x = 0.025$  applied (see Table 6).

Once the simulations are performed, we calculate the thermal conductivity for nine different strains at temperatures 300 K and 600 K using the same procedure as before. The resulting thermal conductivity are plotted as a function of strain in Figure 12.

For both temperatures (300 K and 600 K), our calculated thermal conductivity of PG displays interesting (nonmonotonic, up-and-down) behavior for strains ranging from 0% to 12.5%. Above 12.5% strain the thermal conductivity decreases significantly. The observed trends are similar to those reported by Sun [14], who also investigated the thermal conductivity of monolayer PG, although he noticed more pronounced decrease (67% of the initial value above 3.4% strain). This difference might be due to the difference in the method used, as Sun used first-principle

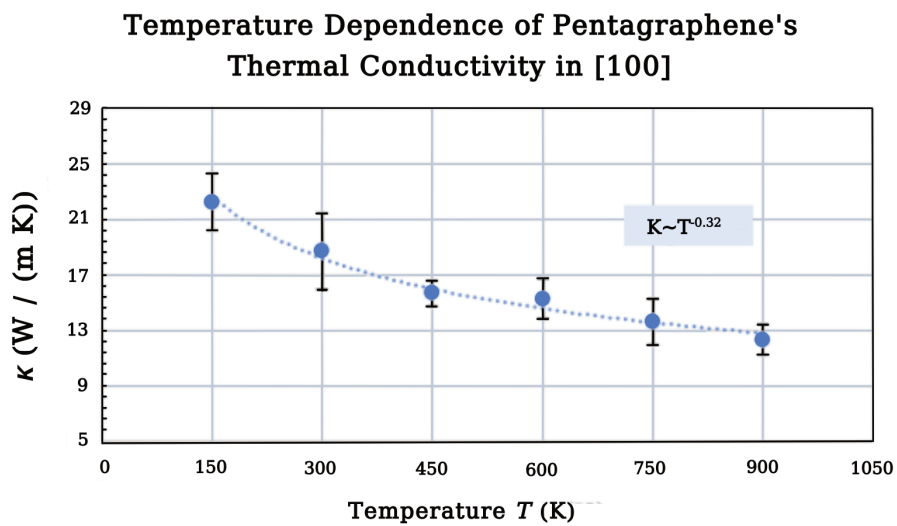


Figure 10. Thermal conductivity of penta-graphene as a function of temperature. The blue curve denotes the best-fitting.

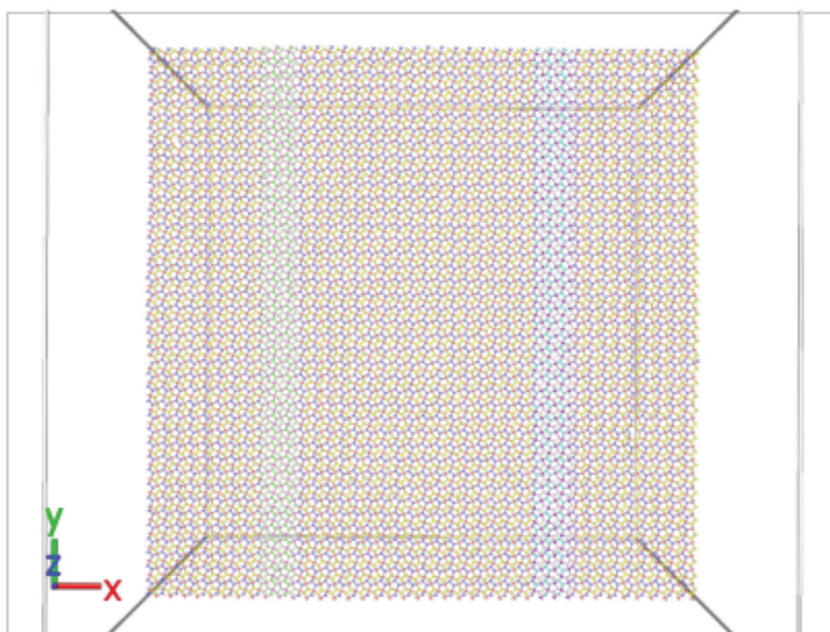
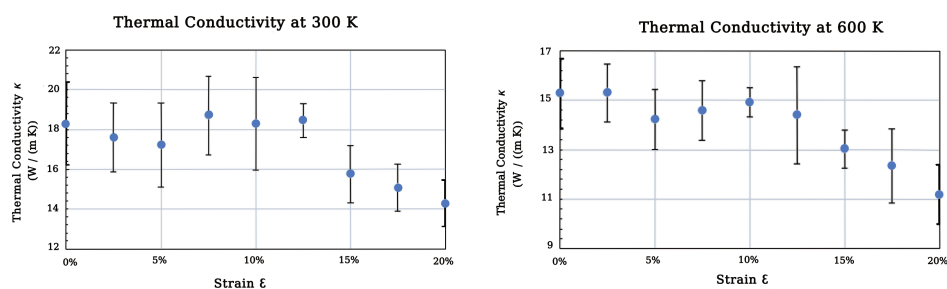


Figure 11. Snapshots of atomic configurations of penta-graphene for temperature of 900 K at the end of NEMD simulation.



**Table 8.** List of lattice constants at 300 K and 600 K with various strains

| Strains (%) | Lattice constants at 300 K (Å) | Lattice constants at 600 K (Å) |
|-------------|--------------------------------|--------------------------------|
| 0           | 3.5995                         | 3.607                          |
| 2.5         | 3.68949                        | 3.69718                        |
| 5           | 3.77948                        | 3.78735                        |
| 7.5         | 3.86946                        | 3.87752                        |
| 10          | 3.95945                        | 3.9677                         |
| 12.5        | 4.04944                        | 4.05788                        |
| 15          | 4.13943                        | 4.14805                        |
| 17.5        | 4.22941                        | 4.23822                        |
| 20          | 4.3194                         | 4.3284                         |

**Figure 12.** Strain Dependence on Thermal Conductivity of PG at 300 K (left) and 600 K (right)

(quantum mechanical) calculations within the framework of the density functional theory (DFT). According to Sun [14] the increasing strain effect was explained by increasing of the phonon lifetimes of specific phonon modes. The reduction of the thermal conductivity was attributed to a decrease in both the phonon group velocity and the phonon lifetime.

#### 4.3. Direction Dependence on thermal conductivity of penta-graphene

In this section, we calculate the thermal conductivity of PG also for the [110] direction, to examine whether or not the heat transport in 2D penta-graphene is isotropic. We use the same method, based on the NEMD simulations combined with the Two Region Method. Here, the simulated system consisted of 28x28 repetitions of the 12-atom unit cell (with sizes  $\sqrt{2}a \times \sqrt{2}a$ ). The  $L_x$  and  $L_y$  sizes of the simulated system were comparable with those used previously (for [100] direction).

We perform similar simulations (as we did in Section 4) to find the temperature dependence for the [110] direction. Once the simulations are performed, we calculate the thermal conductivity for six different temperatures ranging from



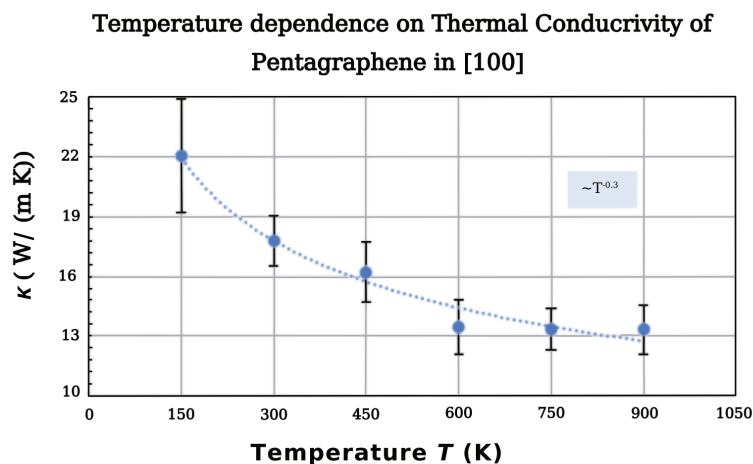


Figure 13. Thermal conductivity of penta-graphene in [110] direction as a function of temperature

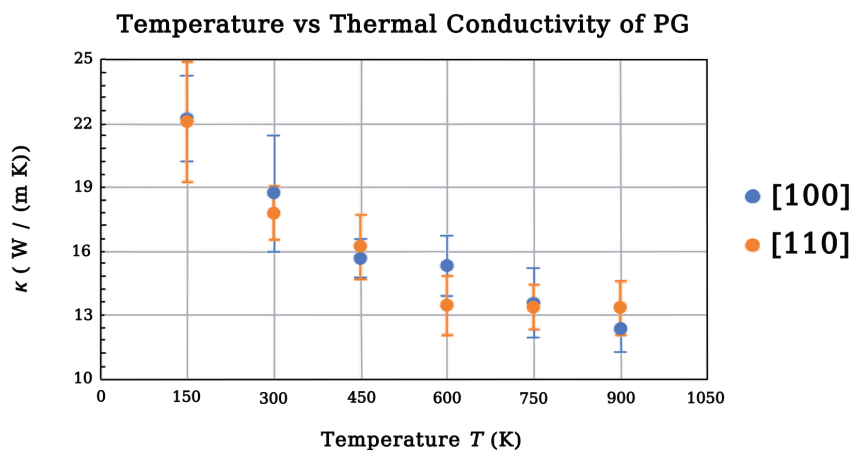


Figure 14. Comparison of thermal conductivities calculated for [100] and [110] directions

150 K to 900 K using exactly the same procedure as we did previously in Subsection 4.1.

The thermal conductivities obtained for [110] direction are plotted as a function of temperature in Figure 13. In Figure 14 we compare thermal conductivities obtained for both studied directions. Surprisingly, it can be seen that the temperature dependence of the thermal conductivity of PG for the [100] and [110] directions is very similar. For the [110] direction, the temperature dependence follows the relation  $\kappa \sim T^{-0.3}$ . At room temperature, the thermal conductivity value is  $18.7 \pm 2.73$  W/(mK) for the [100] direction and  $17.8 \pm 1.27$  W/(m K) for the [110] direction. The subtle difference is, in fact, within the uncertainty. This seems



to show that the thermal conductivity in the penta-graphene sheet is isotropic, meaning that the heat conduction is independent of the heat flow direction. However, it can not be stated unequivocally due to the limitations of our research, mainly the fact that the size-related effects were not investigated.

This statement is supported by the previous research [13] which showed that the thermal conductivity of PG depends on the size of the simulated system. It has been also reported by another similar research [27], which concluded that there is a strong relationship between the size of the simulated system and the determined thermal conductivity. Furthermore, another research [28] has shown that the lattice thermal conductivity of penta-graphene decreases largely when the system size is increased.

## 5. Conclusions

In this paper the thermal conductivity of penta-graphene (PG) was intensively investigated via NEMD simulations combined with the Two Region Method. The optimized Tersoff potential formula was used to describe the interaction between atoms within this fascinating carbon allotrope.

Our investigations show that the thermal conductivity of PG decreases with the increasing of temperature. At the room temperature of 300 K, our calculated thermal conductivity of PG (determined for the [100] direction) is about 18.7 W/(m K), which is much lower than 167 W/(m K) obtained by Xu [13]. This difference is due to the different interatomic potential used (we applied the optimized Tersoff potential to describe the interaction between atoms, while Xu employed the original Tersoff [18] potential).

Interestingly, when we rotated the PG structure by 45 degrees and performed the measurement in the [110] direction (but for the same system size and the same temperature), there was no noticeable difference in the calculated thermal conductivity. This finding shows that the thermal conductivity in penta-graphene is isotropic, meaning that the heat conduction behavior is independent of the heat flow direction.

For the strain effect on the thermal conductivity of PG, in this paper, we performed a simulation at the temperatures of 300 K and 600 K. The calculated result shows that the thermal conductivity of PG has interesting nonmonotonic up-and-down behavior and the result is similar to the investigation of the strain dependence on the thermal conductivity of monolayer PG by Sun.

Our investigation highlights the fascinating thermal transport properties of penta-graphene. The ultra-low thermal conductivity of PG compared to graphene, and the decreasing thermal conductivity of PG with increasing temperatures make PG a great potential material to increase the figure of merit in thermoelectric applications. Furthermore, penta-graphene can withstand strains as high as 20% and it is expected that PG will be a good candidate in nanomechanics applications. We hope that these findings made by means of simulations will become a bridge to inspire and encourage experimental works, especially in the synthesis of PG.



## Appendices

### *Appendices A. Input Files*

#### *Appendix A1. Initial Simulation*

```
dimension      3
boundary       p p p

units          metal
atom_style     atomic

read_data      penta_graphene.data

pair_style     tersoff
pair_coeff     * * penta.tersoff C C C

mass          1 12.0
mass          2 12.0
mass          3 12.0

timestep       0.0005
fix           1 all npt temp 150.0 150.0 0.1 &
              x 0.0 0.0 1.0 &
              y 0.0 0.0 1.0 &
              couple none

velocity       all create 150.0 12345 rot yes mom yes

thermo         100
thermo_style   custom step temp press lx ly

dump           myDump all custom 100 dump.lammpstrj.* id type x y z

run           120000
```

*Appendix A2. Main Simulation (Two Region Method)*

```

variable      kB      equal 0.00008617

variable      seed_1 equal 12312
variable      seed_2 equal 45623
variable      seed_3 equal 78934

variable      t       equal 300.0
variable      tlo     equal 280.0
variable      thi     equal 320.0
variable      tdamp   equal 0.5

variable      n_steps_stage_1 equal 10000
variable      n_steps_stage_2 equal 50000
variable      n_steps_stage_3 equal 100000

variable      n_thermo equal 10
variable      n_dump   equal 100

dimension     3
boundary      p p f
units         metal
atom_style    atomic
read_data     penta_region_300K.data

pair_style    tersoff
pair_coeff    * * penta.tersoff C C C C C C C C C

mass          1 12.0
mass          2 12.0
mass          3 12.0
mass          4 12.0
mass          5 12.0
mass          6 12.0
mass          7 12.0
mass          8 12.0
mass          9 12.0

group         left  type 4 5 6
group         center type 1 2 3
group         right type 7 8 9

timestep      0.0005
dump          my_dump all custom ${n_dump} dump.lammpstrj id type x y z
velocity      all create ${t} ${seed_1} dist gaussian

compute       Tleft left temp
compute       Tright right temp

```

```

# --- 1st stage ---
# 1st equilibration run
fix          nvt_fix all nvt temp ${t} ${t} ${tdamp}
thermo       ${n_thermo}
run          ${n_steps_stage_1}

timestep     0.0005
unfix       nvt_fix
reset_timestep 0

# --- 2nd stage ---
# 2nd equilibration run

fix          nve_fix all nve
fix          left_thermostat left langevin ${tlo} ${tlo} ${tdamp} &
            ${seed_2} tally yes
fix          right_thermostat right langevin ${thi} ${thi} ${tdamp} &
            ${seed_3} tally yes

fix_modify   left_thermostat temp Tleft
fix_modify   right_thermostat temp Tright

variable     tdiff equal c_Tleft-c_Tright
thermo_style custom step temp c_Tleft c_Tright &
            f_left_thermostat f_right_thermostat v_tdiff
thermo       ${n_thermo}
run          ${n_steps_stage_2}

# --- 3rd stage ---
# thermal conductivity calculation

# reset langevin thermostats to zero energy accumulation
unfix       left_thermostat
unfix       right_thermostat

fix          left_thermostat left langevin ${tlo} ${tlo} ${tdamp} &
            ${seed_2} tally yes
fix          right_thermostat right langevin ${thi} ${thi} ${tdamp} &
            ${seed_3} tally yes

fix_modify   left_thermostat temp Tleft
fix_modify   right_thermostat temp Tright

fix          ave all ave/time 10 100 1000 v_tdiff ave running
thermo       1000
thermo_style custom step temp c_Tleft c_Tright &
            f_left_thermostat f_right_thermostat v_tdiff f_ave

compute     ke all ke/atom
variable     temp atom c_ke/(1.5*${kB})

```

```

compute      layers all chunk/atom bin/1d x lower 1.82 units box
fix          temp_profile all ave/chunk 10 100 1000 layers &
              v_temp file profile.langevin
run          ${n_steps_stage_3}

```

## References

- [1] Novoselov K S, Geim A K, Morozov S V, Jiang D, Zhang Y, Dubonos S V, Grigorieva I V and Firsov A A 2004 *Science* **306** (5696) 666
- [2] Bucknum M J and Hoffmann R 1994 *J Am Chem Soc* **116** (25) 11456
- [3] Malko D, Neiss C, Viñes F and Görling 2012 *Phys Rev Lett* **108** (8) 86804
- [4] Zhang S, Zhou J, Wang Q, Chen X, Kawazoe Y, and Jena P 2015 *Proc. Natl. Acad. Sci. USA* **112** (2372) 2372
- [5] Einollahzadeh H, Dariani R S and Fazeli S M 2016 *Solid State Commun.* **229** 1
- [6] Yu Z G and Zhang Y W 2015 *J. Appl. Phys.* **118** (16) 165706
- [7] Wang Z, Dong F, Shen B, Zhang R, Zheng Y, Chen L, Wang S, Wang C, Ho K, Fan Y J, Jin B Y and Su W S 2016 *Carbon* **101** 77
- [8] Quijano-Briones J J, Fernandez-Escamilla H N and Tlahuice-Flores A 2016 *Phys. Chem. Chem. Phys.* **18** 15505
- [9] Berdiyrov G R, Dixit G and Madjet M E 2016 *J. Phys. Condens. Matter* **28** (47) 475001
- [10] Li X, Zhang S, Wang F Q, Guo Y, Liu J and Wang Q 2016 *Phys. Chem. Chem. Phys.* **18** 14191
- [11] Guo Y, Wang F Q and Wang Q 2017 *Appl. Phys. Lett.* **111** 73503
- [12] Xiao B, Li Y C, Yu X F and Cheng J B 2016 *ACS Appl. Mater. Interfaces* **8** 35342
- [13] Xu W, Zhang G and Li B 2015 **143** (15) 154703
- [14] Sun Z, Yuan K, Zhang X, Qin G, Gong X and Tang D 2019 *Physical Chemistry Chemical Physics* **21** (28) 15647
- [15] Hoover W G and Hoover C G 2005 *Condensed Matter Physics* 247
- [16] OVITO - The Open Visualization Tool 2019 <http://www.ovito.org/>
- [17] Winczewski S, Shaheen M Y and Rybicki J 2018 *Carbon* **126** 165
- [18] Tersoff J 1989 *Phys. Rev. B* **39** 5566
- [19] Tersoff J 1990 *Phys. Rev. B* **41** 3248
- [20] Erhart P, Albe K 2005 *Phys. Rev. B* **71** 35211
- [21] Winczewski S and Rybicki J 2019 *Carbon* **146** 572
- [22] Tersoff J 1988 *Phys. Rev. B* 6991
- [23] Sandia Corporation 2019 *LAMMPS Documentation*
- [24] VMD – The Visual Molecular Dynamics 2020 <https://www.ks.uiuc.edu/Research/vmd/>
- [25] GNUPlot 2020 <http://www.gnuplot.info/>
- [26] Wu X, Varshney V, Lee J, Zhang T, Wohlwend J L, Roy A K and Luo T 2016 *Nano Lett.* **16** (6) 3925
- [27] Zhang Y Y, Pei Q X, Cheng Y, Zhang Y W and Zhang X 2017 *Computational Materials Science* **137** 195
- [28] Wang F Q, Yu J, Wang Q, Kawazoe Y and Jena P 2016 *Carbon* **105** 424
- [29] Muller-Plathe F 1997 *J. Chem. Phys.* **106** 6082
- [30] Li J and Lee J D 2014 *Acta Mechanica* **225** (4-5) 1223
- [31] Cao A 2012 *Journal of Applied Physics* **111** (8) 83528